


Fano interference in nanoscale bismuth constrictionsAvner Niv, Ping'an Li, Tal Oz, Tilman König , and Yoram Selzer ^{*}*Department of Chemical Physics, School of Chemistry, Tel Aviv University, Tel Aviv 69978, Israel*

(Received 21 July 2021; revised 9 November 2021; accepted 2 December 2021; published 21 December 2021)

We report on electrical transport measurements of ballistic Bi constrictions with top and bottom gate electrodes in which interference of their metalliclike surface states and quantized bulk states results in Fano resonance features in the conductance. Within the formed constrictions, the mean spacing between the bulk states is smaller than their coupling to the leads. Under these conditions, gradual lapses in the scattering phases of the bulk states in response to a change in the gate voltage are inferred by analyzing the symmetry parameter of the Fano features. Comparison between the results of this analysis in response to the top and bottom gates also suggests that the surface states are localized at the interface between the Bi and the underlying SiO₂ layer. Our findings advocate that nanofabrication of Bi could better harness its unique electronic properties to impart advanced functionalities.

DOI: [10.1103/PhysRevB.104.235140](https://doi.org/10.1103/PhysRevB.104.235140)**I. INTRODUCTION**

Bismuth (Bi) is characterized by a very small effective mass [1] of its bulk charge carriers. This property becomes apparent in angle-resolved photoemission spectroscopy (ARPES) of ultrathin Bi(111) films, in the form of quantized (bulk) well states (QWSs) at the $\bar{\Gamma}$ and \bar{M} points of the Brillouin zone with energy spacing that depends on the thickness of the films [2–4]. Considering also the long mean free path [5] and the strong spin-orbit coupling [6] of these bulk carriers, nanostructured Bi is vital for the study of quantum size effects [1] and highly attractive for applications such as spintronics [7] and thermoelectrics [8].

The ARPES measurements also show that the $\bar{\Gamma}$ and \bar{M} points are bridged by (Rashba spin-split) surface states bands (SS1 and SS2) with carriers that have a higher effective mass than in the bulk [9,10], making nanoscale Bi structures less prone to quantum confinement than had previously been suggested [8,11]. Temperature-dependent conductance measurements of ultrathin Bi films initially suggested that at sufficiently low temperatures the contribution of the bulk states can be thermally quenched leaving only the surface states to dominate the transport properties [12–14]. Yet, since the surface and bulk states coexist within the same system and since the decay length of the former states into the bulk is not negligible and also depends on their in-plane momentum [15,16], the electronic structure of quantum confined Bi has to be more intricate. Indeed, ARPES measurements show hybridization of the SS1 and SS2 bands with conduction and valence bulk states, respectively, around the \bar{M} point [3,4]. This hybridization is also revealed in magnetotransport measurements, which although they postulate a metallic behavior at low temperatures for films thinner than 25 bilayers (1BL = 3.93 Å) [16–20], also identify signatures of bulk-associated coherent transport (in the form of weak antilocalization) in addition to the incoherent surface-associated scattering [16,20].

This observation is supported by nonlinearities in the Hall resistivity of the films [21], which like in other Bi-based topological films [22–24] imply coherent interaction between the QWSs and surface transport channels. The Hall measurements also show that the thickness-dependent QWS contribution to transport has mainly an electron character [21]. Considering band structure data and calculations [4,25], the involved electrons originate in the electron pocket near the \bar{M} point, with negligible contribution of the pocket near the $\bar{\Gamma}$ point. Thus, while QWSs from the conduction band at the \bar{M} point are unoccupied for very thin films due to quantum confinement, with increasing thickness (and less confinement), at around 30 BL, these bulk levels are starting to cross the Fermi level and to overlap energetically with and couple to the surface states.

Here we exploit the above coherent coupling between surface and quantized bulk states to impart Fano resonance in the electrical conductance of nanoscale ballistic Bi constrictions. The Bi constrictions described and discussed below are all, similarly to previously studied films, (111) oriented, however, with an additional (large) lateral confinement formed by lithography. Careful control of the measured structures ensures that in all of them a single grain is located within the confined feature. One can regard them as if we zoom in on one grain in the previously measured films, however, with an additional confinement, that results in a more pronounced quantization of the bulk levels. Due to the much larger effective mass of the surface states, the effect of confinement on these states is negligible, leaving them as an affecting continuum. Under such conditions within features that are smaller than the phase length of Bi, Fano resonance is taking place.

Fano resonance, which is the interference between a resonant state and a continuum, appears ubiquitously in various systems. In meso- and nanoscale electronic systems it has been observed in the transport properties of various quasi-one-dimensional (1D) systems such as single magnetic atoms [26], single electron transistors [27], quantum dots [28–30], carbon nanotubes [31], artificial molecules [32], and Weyl semimetal nanowires [33]. Recently, Fano resonance was suggested for the detection of the Majorana bound state [34]. Specifically,

^{*}selzer@tau.ac.il

our work corresponds with the Fano resonance observed in the Weyl nanowires [34], with an opposite role of the surface and bulk states. While in Weyl nanowires the confined states are formed at the surface and the bulk serves as the continuum, here it is the bulk states that are sufficiently confined to be quantized.

The conductance in all these systems, based on the Landauer-Büttiker formalism, with a continuous nonresonant background conductance G_{bg} and a single discrete resonant level located at ε_0 and coupled to the leads by Γ has the following expression [35]:

$$G(\varepsilon) = G_{inc} + G_{bg} \frac{1}{1 + q^2} \frac{(\tilde{\varepsilon} + q)^2}{\tilde{\varepsilon}^2 + 1}, \quad (1)$$

where $\tilde{\varepsilon} = (\varepsilon - \varepsilon_0)/(\Gamma/2)$ and q is an asymmetry parameter. For $q \rightarrow \infty$, Eq. (1) becomes the Breit-Wigner form, while for $q = 0$, it shows an antiresonance dip. Between these two limits, varying the value of q produces the entire family of Fano line shapes. All background incoherent contributions to the conductance are inserted into G_{inc} . The two parameters, $\tilde{\varepsilon}$ and q , can be associated with phase shifts involved in the scattering process [33]. The parameter q is associated with a nonresonant phase by $\theta = \cot^{-1}(|q|) - (\pi/2)$, and $\tilde{\varepsilon}$ is associated with a resonant phase according to $\tan \theta_0 = -\Gamma/2(\varepsilon - \varepsilon_0)$. The latter varies from zero to π as the energy is moved through the resonance from below [35].

Previous reports of ballistic Bi structures focused on the subquantum regime of conductance [36,37] and on the topological transport properties of 1 BL thick layers of Bi(111) [38]. Fano resonance has not been observed in all these former studies due to lack of continuum and quantized states, respectively. By demonstrating Fano resonance in quantum confined Bi structures, we provide additional insight into their intriguing electronic structure. Specifically, we show that analysis of the Fano features implies dynamical effects in the transport properties of nanoconfined Bi, which bear significant resemblance to processes previously observed in quantum dots with small mean level spacing [39–42]. Analysis of the Fano asymmetry parameter can semiquantify the scattering phases of the bulk states. We further note that the observed Fano resonance could explain previous highly efficient thermopower measurements of Bi nanowires and therefore could open routes for efficient heat harvesting capabilities [43].

II. EXPERIMENTAL DETAILS

Bi structures, 25 nm thick, were patterned by e -beam lithography followed by thermal evaporation resulting in constrictions with a width of 25 nm such as in Fig. 1(a). The structures were fabricated on top of (highly doped) Si substrates covered with 60 nm of a gate oxide. Since a 2–3 nm thick natural Bi oxide layer covers the formed Bi structures, the effective cross section of the constrictions is $\sim 22 \text{ nm} \times 20 \text{ nm}$. This has been verified by transmission electron microscope (TEM) images. All devices were annealed under vacuum at 150 °C prior to measurements, using the covering Bi oxide as a scaffold that imparts mechanical stability which inhibits dewetting [44,45] at elevated temperatures and smearing of the features due to surface diffusion. The geometry

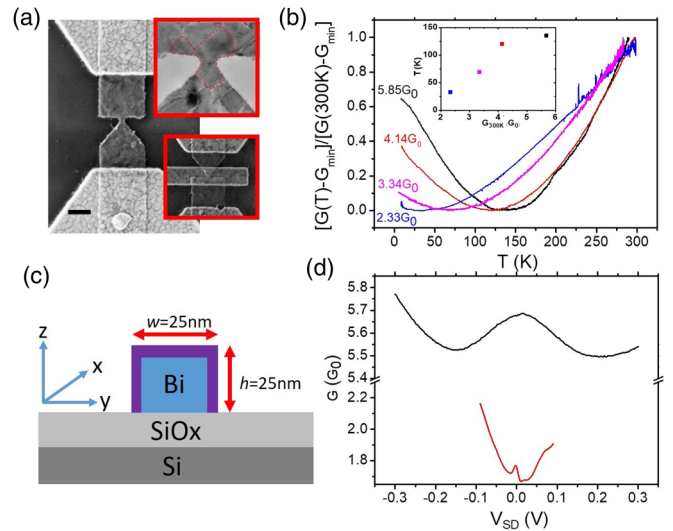


FIG. 1. The effect of temperature on conductance. (a) An SEM image of a Bi device with Au contacts on both sides. Scale bar is 100 nm. Top inset: A TEM image showing the grain boundaries around a 25 nm constriction. Bottom inset: An SEM image of a device with a top (Au) gate. (b) Normalized conductance, for several devices with indicated G_{300K} values, as a function of temperature. The corresponding values of G_{min} (in units of G_0) are 5.4, 3.97, 3.33, and 1.44. Inset: Temperature of minimum conductance as a function of G_{300K} . (c) The geometry of a cross section of a constriction used for the calculations of the density of states. The Bi oxide layer (in purple, not drawn to scale) is 2–3 nm thick based on TEM images. Conduction is parallel to the x direction. (d) Conductance of the $5.85G_0$ and $2.33G_0$ devices in (b) as a function of V_{SD} at 8 K.

of the used constrictions results in structures with 100–200 nm grains, all with a [111] orientation, which span the constrictions of the devices, as demonstrated in the TEM image in the inset of Fig. 1(a). Ohmic contacts to Au leads were established after locally stripping the covering oxide [43]. Based on four-probe measurements of Bi wires formed similarly to the features used here, we prove that the leads in the two-terminal geometry establish Ohmic contacts to the Bi and that the approximated ballistic length is $\sim 80 \text{ nm}$, i.e., longer than the constrictions. See more details in the Supplemental Material [46]. For some devices, a top gate was also fabricated [see inset in Fig. 1(a)] using the native Bi oxide layer as the gate dielectric.

For conductance measurements, a small alternating source-drain voltage was applied between the leads and the measured preamplified signal was lock-in detected. The conductance was then recorded as a function of V_G , the gate voltage values. For differential conductance measurements, a finite offset source-drain voltage V_{SD} was added and the measured response, $G = dI/dV_{SD}$, to the small alternating drain-source voltage was recorded as a function of both V_G and V_{SD} . Conductance is reported in units of quantum of conductance, $G_0 = 2e^2/h$.

III. RESULTS AND DISCUSSION

Figure 1(b) plots the normalized change in conductance, as a function of temperature, for several devices with different

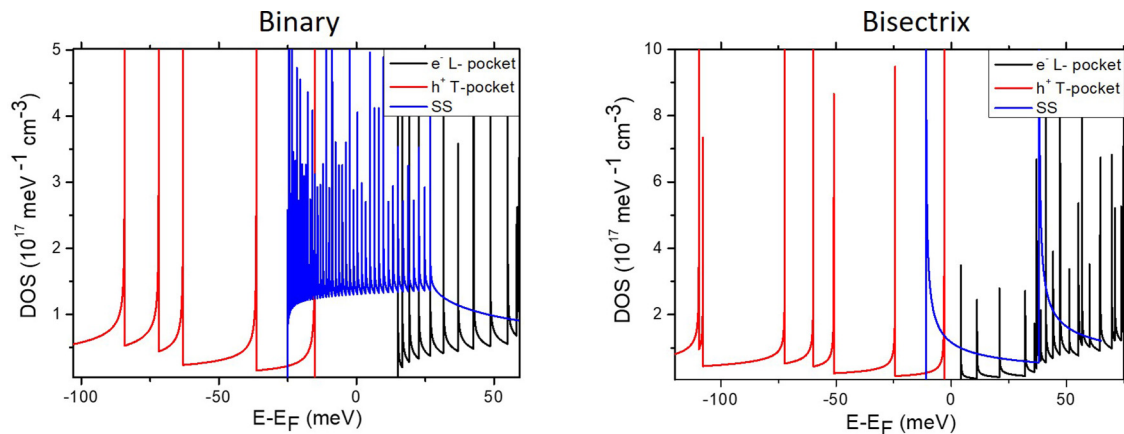


FIG. 2. Calculated density of states for the two considered directions of conduction. Confinement in the y and z directions is according to the geometry in Fig. 1(c).

$G(300\text{ K})$ values. In order to facilitate comparison between the shapes of the curves, the values are plotted on a normalized $[0, 1]$ scale, by plotting $[G(T) - G_{\min}]/[G(300\text{ K}) - G_{\min}]$, where G_{\min} is the minimum conductance value measured for each device. All devices show a transition between a thermally activated semiconductorlike regime with $dG/dT > 0$ at high temperatures and a metallic regime with $dG/dT < 0$ at low temperatures. A similar behavior has been observed in thin films of Bi(111) [14,16]. However, in our devices we note that curves with lower $G(300\text{ K})$ values have a lower transition temperature between the two conductance regimes [inset of Fig. 1(b)] and also a more flat “metallic” behavior, i.e., less prone to temperature change, at low temperatures.

In order to understand this observation it is necessary to account for the fact that unlike thin films, each formed Bi constriction could have a different crystalline orientation in the direction of conduction. Since the mass tensor of the charge carriers in Bi is highly anisotropic [8,47,48], this variation in crystalline orientation leads to a variation in the quantum confined electronic structure of the constrictions. To semiquantify this effect we calculate (see Supplemental Material [46]) the bulk and surface density of states for two Bi [111] constrictions with identical cross sections as in Fig. 1(c) and assuming transport (in the x direction) parallel to either the binary or the bisectrix directions of the crystal.

When using the calculated density of states (Fig. 2) to understand the measurements in Fig. 1(b), it is important to emphasize that they represent two extreme (perpendicular) orientations and that formed constrictions could have other density of states, *between these two extremes*. Further, the calculations do not consider broadening of the electronic levels due to coupling to the leads. As will be shown below, this broadening can be experimentally determined and it has a subtle effect on the unique transport properties of the devices.

For the considered geometry, the Binary direction has a $\sim 25\text{ meV}$ gap for the bulk states, bridged by a relatively high density of surface metallic modes. The effect of temperature on a device of this type, with a relatively large bulk gap and several surface modes, can explain the $5.68G_0$ curve in Fig. 2. At $T = 300\text{ K}$, albeit thermal excitation, because of the relatively large band gap the contribution of the surface states to transport is more dominant than that of the bulk states.

With decreasing temperature, conduction through the bulk states is further thermally quenched leaving only the surface states to contribute to transport with increasing efficiency as the temperature decreases due to less electron-phonon scattering (the surface Debye temperature of Bi is estimated to be 47 K) [49].

In contrast, devices with constrictions that are more bisectrix oriented have a smaller band gap and as a result a lower transition temperature between the two conductance regimes. They also have a smaller number of surface metallic modes, which start to affect the nature of conductance only at low temperatures. In order to understand their transport properties, it is imperative to consider the surface to bulk scattering time, τ_{sb} and the phase coherence time τ_{ϕ} in such constrictions [50]. When $\tau_{\text{sb}}/\tau_{\phi} < 1$, charge carriers scatter between the bulk and surface states while remaining coherent, and therefore the two conducting channels can be regarded as one coherent channel. In the opposite regime, when $\tau_{\text{sb}}/\tau_{\phi} > 1$, the carriers lose coherence before being scattered and the two channels are separable and independent. With decreasing temperature, since the band gap in these constrictions is small, transport continues to have contributions from both surface and bulk modes. Therefore, with decreasing temperature, as the phase coherent length and as a result also τ_{ϕ} increase making $\tau_{\text{sb}}/\tau_{\phi}$ smaller, the coherent behavior of the system increases and correspondingly, the temperature-dependent incoherent metallic behavior is lost. Thus in such constrictions, the apparent less metallic behavior is due to a more pronounced coherent coupling between bulk and surface modes.

The above reasoning is further elaborated in the conductance curves in Fig. 1(d) measured at 8 K as a function of V_{SD} . The high (black) conductance curve, as discussed above, is associated with a constriction that has a more binary-oriented nature, i.e., a relatively large band gap and a high number of surface modes. Therefore, its transport properties at 8 K bear mainly a metallic nature and the observed decrease in conductance, as V_{SD} departs from zero value in both polarities, is due to continuous heating by phonon emission because of inelastic scattering events. The conductance starts to increase again when the applied bias brings the bulk states into the energy window between the two Fermi levels in the leads. In contrast, we associate the narrow peak around zero bias

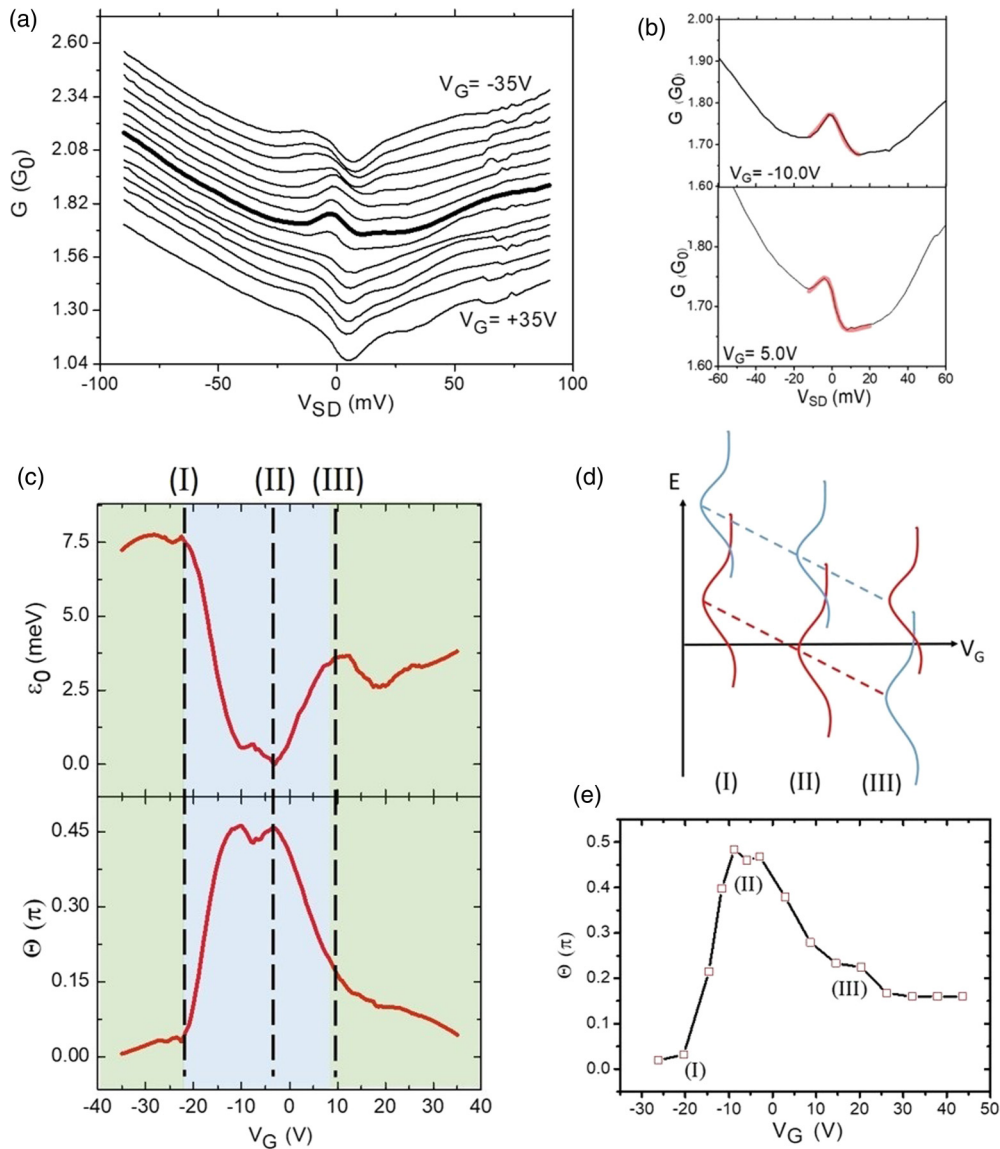


FIG. 3. Fano resonance in response to bottom V_G . (a) Conductance curves as a function of bottom V_G , varied in steps of 5 V measured at 8 K. The curves are shifted for clarity and the curve corresponding to bottom $V_G = 0$ V is shown in bold. (b) Fitting of the Fano equation to selected conductance curves at the indicated V_G values. (c) ε_0 and θ as a function of bottom V_G extracted from the fittings of Eq. (1) to the conductance curves. (d) A schematic model showing the resonance level (red) with energy ε_0 and a background overlapping resonance level (cyan) with energy ε_1 , which contributes to the Fano parameter q . The levels alignments marked by (I–III) correspond to the vertical lines in (c) with the same markers. Note that at (III), when ε_0 is below the Fermi energy the role of the levels is exchanged and ε_1 becomes the resonant level (changing its color to red). (e) Calculated phase based on the model as explained in the text.

in the low (red) conductance curve with coherent processes resulting from the fact that the bulk gap is small and the energy of the surface and bulk levels is close. This peak, as in other low ($\sim 2G_0$) conductance devices, appears to be affected by an applied gate voltage, V_G , resulting in Fano-like features. Here, we analyze and compare between the Fano-resonance responses in one device for which a response to both the top and bottom gates could be simultaneously measured. We choose a low conductance device ($\sim 2G_0$), which can be quantitatively analyzed based on Eq. (1), which assumes only one resonance level. We note that what appear to be Fano features are also observed with higher conductance devices; however, their analysis will be discussed elsewhere.

Figure 3(a) depicts several conductance curves as a function of *bottom* V_G with a dip-peak-dip transition around zero bias as bottom V_G is scanned between +35 V and –35 V.

The peaks and dips in each of these curves are well fitted by Eq. (1) in the range $|V_{SD}| \leq 20$ mV as demonstrated in Fig. 3(b). For all fitting curves the coupling to the leads is $\Gamma = 16$ meV. The values of ε_0 and θ extracted from these fits as a function of bottom V_G are shown in Fig. 3(c). ε_0 is reported versus the Fermi energy (E_F) at zero bias and θ as a difference from the minimal extracted value in order to emphasize the change of phase.

For gate values of $V_G \leq -20$ V, the resonance level according to Fig. 3(c) appears not to be affected by the applied gate

field and instead to hover at the same energy position. With more positive V_G values, between the vertical lines marked with (I) and (II) in Fig. 3(c), a downshift of the resonant level is inferred accompanied by an increase of the background phase, θ . At $V_G \sim -10$ V, the quantized resonance level becomes aligned with E_F and an almost $\pi/2$ background phase shift is accumulated leading to a peak in the conductance curves [in Fig. 3(a)]. As V_G becomes more positive, between the (II) and (III) lines, an apparent decrease in phase comes with a shift of the resonance level to a higher energy. Above $V_G \sim 10$ V, the resonance level parks at a constant value with negligible background phase change and a deep appears once again in the measured conductance [Fig. 3(a)].

We focus first on a possible explanation for the behavior of θ (calculated from q). In previous studies of Fano systems, changes in this phase were induced by a magnetic field in Aharonov-Bohm interferometers [30] and by Coulomb interaction within the quantized states of a coupled quantum dot by means of a gate voltage [28]. Here the phase also appears to depend on V_G , however, without any apparent charging effects. In order to explain the phase behavior we note that the formed Bi constrictions bear an important similarity with large quantum dots, for which both the magnitude and the phase of transmission through the levels of the dots were measured [39–42,51]. These former measurements also showed Fano-like features, which were analyzed by considering the fact that the mean level spacing in these dots was smaller than their coupling to the leads [39–42]. Such conditions, based on our calculations, also prevail here. The energy difference between the quantized bulk levels (Fig. 2) is estimated to be ≤ 10 meV, while based on the fitting to the Fano model using Eq. (1), the coupling to the leads is $\Gamma = 16$ meV.

Under such conditions, transport through each of the quantized bulk resonance levels interferes, in addition with the surface continuum, and also with other resonance (background) states. The nature of this interference depends on their position and width and its final outcome is a change in q [52].

Based on this general model of overlapping background resonance levels, Fig. 3(d) outlines schematically a suggested scenario that can explain the apparent background phase behavior in response to the bottom gate. Qualitatively, the scenario assumes a resonance level (associated with ε_0) and an overlapping resonance state (with energy ε_1). As bottom V_G becomes more positive, all levels are shifting down in energy. Between the vertical dashed lines (I) and (II), ε_0 is made to align with the Fermi level and the background phase increases due to an increase in the phase associated with ε_1 , as this level becomes also closer to the Fermi level. With further increase of V_G , between the vertical dashed lines (II) and (III), destructive interference between the two overlapping resonances leads to a decrease in the apparent background phase. At (III), ε_0 is completely moved away from the bias window between the two Fermi levels of the leads and the previously background resonance level, ε_1 , becomes the new resonance level [hence the change in color from red to cyan in Fig. 3(d) at this point].

To quantify the suggested scenario, we use a previously suggested treatment of Fano systems with overlapping levels [51]. To a first approximation, the effect of a background state with energy ε_i and coupling Γ_i on the Fano resonance

shape can be accounted for as an additional phase term in Eq. (1) according to $\theta_i(\varepsilon) = -\cot^{-1}[2(\varepsilon - \varepsilon_i)/\Gamma_i]$. As a result, the experimentally determined asymmetry parameter effectively becomes

$$q = -\cot(\Theta) = -\cot\left(\theta + \sum_i \theta_i\right). \quad (2)$$

The calculated background phase in Fig. 3(c) was calculated assuming a resonance level, located initially at $\varepsilon_0^{\text{initial}} = 8$ meV, and a background quantized level $\varepsilon_1^{\text{initial}}$ located at 16 meV. We find that for all levels a width of $\Gamma = 16$ meV gives accurate results. The spacing between levels should be according to the model [52] within the resonance width. The used number of 8 meV is on par with the calculated level spacing as discussed in the Supplemental Material [46]. The response of each of these levels to V_G is $\varepsilon_i = \varepsilon_i^{\text{initial}} - \alpha(V_G - V_G^0)$, where α is the lever arm of the gate voltage and is used here as a free parameter to adjust the model to the applied V_G range, using V_G^0 as the initial gate voltage for the fitting. To simplify the analysis, we use only one background resonant level. The phases are subsequently calculated in the following way: for each V_G value a calculated ε_1 [$\varepsilon_1 = 16$ meV $-\alpha(V_G - V_G^0)$], is used to calculate an additional background phase, $\theta_1(\varepsilon) = -\cot^{-1}[2(\varepsilon - \varepsilon_1)/16$ meV], for each energy value in the range $|\varepsilon| \leq 20$ mV, i.e., the potential window used for the fitting of Eq. (1). This set of phases, transformed into q values by Eq. (2), is inserted into Eq. (1) to form transmission curves. These curves were subsequently fitted by a *single* q value using Eq. (1) and the position of the resonance state ε_0 . The phase values resulting from the calculation are reported in Fig. 3(e) as a function of bottom V_G . The apparent similarity to the experimental results suggests that the used model captures the important features of the transport characteristics within the blue region in Fig. 3(c). It does not, however, explain why within the green regions of this figure, the resonance level position does not depend on the applied gate voltage. This behavior is also observed in the response of the same device to a top gate. Figure 4 plots this response as *top* V_G changes between -0.5 and $+0.5$ V.

According to Fig. 4(c), ε_0 in response to top V_G is also not shifting monotonously with V_G . There are V_G regions, such as between the vertical dashed lines (I) and (II), in which ε_0 is decreasing and θ is increasing, and in other gate voltage regimes, such as between lines (II) and (III), in which ε_0 is hovering at a certain value while θ is decreasing.

Based on the model of overlapping background resonance levels, Fig. 4(d) outlines a suggested scenario that can explain the apparent phase behavior. The model needs to only explain the marked blue region in Fig. 4(c), as we regard the similar phase and energy patterns appearing in the other (green) regions as a duplication of the blue-region behavior but with a resonance level, ε_0 , parking at different values with respect to the Fermi level at zero bias [upper panel in Fig. 4(c)].

Qualitatively, the scenario assumes a broad resonance level (associated with ε_0), hovering near the zero-bias Fermi level with hardly any effect of V_G on its position. In addition, there is an overlapping (narrower) resonance state (with energy ε_1), that has a steeper gate-dependent energy behavior. As V_G becomes more positive, the narrow level is shifting down in

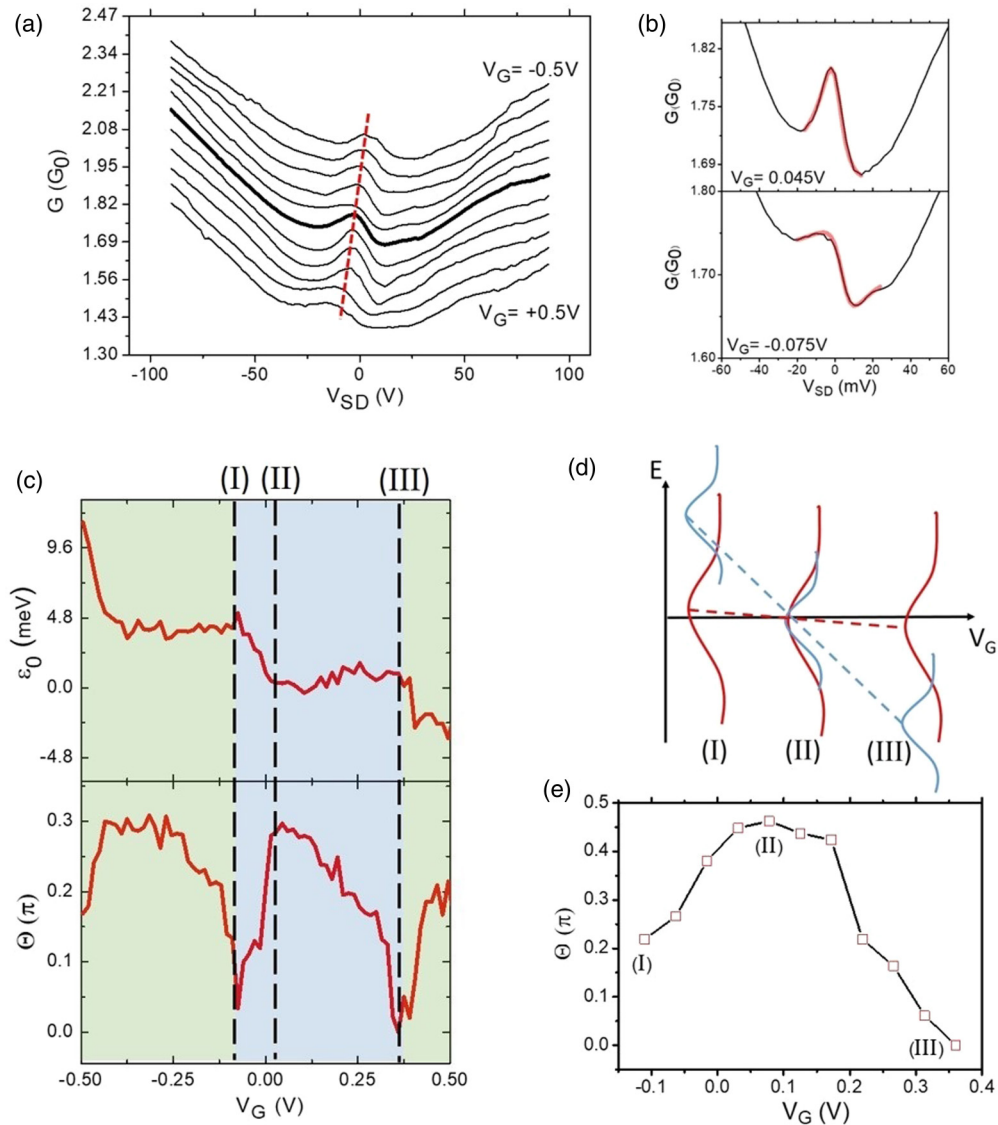


FIG. 4. Fano resonance in the same device as a function of top V_G . The contents of the different panels are explained in Fig. 3.

energy crossing the broad level. Between the vertical dashed lines (I) and (II), the background phase increases due to an increase in the phase associated with ε_1 , until both levels are energy aligned. Beyond this point, the destructive interference between the two overlapping resonances leads to a decrease in the apparent background phase.

A similar procedure to quantify the model results in the phase behavior plotted in Fig. 4(e), which also resembles quite well the experimental data (within the blue region).

Several important points regarding the suggested model need to be discussed. The width difference between the two used resonance states could in general result from level attraction due to, for example, coupling to the continuum [52]. Under such conditions, some of the states are (partially) decoupled from the continuum and become long lived (narrow resonance), while others become short-lived states (broad resonance). The former states, with their long-lived localized charge, respond more steeply to the gate voltage. In our system, considering the density of states in Fig. 2, the broad level could also be associated with a surface state and the narrow

level with one of the quantized bulk states. Thus, in this case the gate also affects the position of the Fano continuum, which in this case is a broad surface state.

At this stage, it is difficult to understand the experimental behavior of ε_0 as a function of V_G . The model, which pins ε_0 and seems to capture the overall apparent phase behavior, is probably not sufficiently subtle to follow the dynamics of ε_0 and more elaborate scenarios are needed. For example, it can be explained by electrostatic screening of the bulk states from the gate by the surface states [53] where as V_G becomes more positive, screening decreases to a point where eventually ε_0 is shifted. Alternatively, models formerly invoked to explain phase lapses in quantum dots [39–42] can be used. These models consider Coulomb interactions between levels as well as population switching events [54]. In this case, broad and narrow levels swap their position and respective occupancies as a function of the gate voltage. Additional work is needed to identify the relevant mechanism here.

We do note, however, that a similar Coulomb repulsion effect causing a shift of levels has recently been suggested

to explain metal-insulator transition in Bi films [4] and could be operative here under a gate field. While in quantum dots, these Coulomb repulsion effects result in instantaneous phase lapses, here phase variations are gradual. This perhaps can be explained by coupling of the resonant levels to several trajectories (modes) of the continuum [55].

A comparison between the effects of the two applied gate voltages V_G on the position of the levels as revealed in Figs. 3(d) and 4(d) might shed light on where the surface states that participate in the measured coherent processes are physically located within the formed structures. The top gate, which due to its very thin dielectric is expected to be more electrostatically effective, does not affect the levels associated with the surface states [red levels in Fig. 4(d)]. In contrast, the bottom gate appears to shift all levels. This implies that the surface states are localized at the interface between the Bi features and the underlying SiO_2 substrates. As a result, they can be affected by the (near) bottom gate but due to screening within the bulk Bi, do not electrostatically “feel” the top gate. This conclusion is supported by previous observations. Surface oxidation of Bi has been shown to deteriorate surface states and decrease their conductance [19], and in contrast,

capping [14,15] and encapsulation [7,56–58] of Bi surfaces by other oxides does maintain coherent surface states transport. Theoretical understanding of all these observations is only starting to emerge [59,60].

IV. CONCLUSIONS

The above results show that quantum confined ballistic Bi structures can be used to harness their unique electronic structure to impart advanced transport properties. Specifically, coherent coupling between surface and bulk states results in Fano resonances under quantum confined and ballistic conditions with gate-dependent asymmetry parameters. Work is under progress to harness these findings for thermoelectric applications [61,62].

ACKNOWLEDGMENTS

Support by the Israel Science Foundation (Grant No. 1059/18) and the Schmidt Futures foundation (via a breakthrough science grant) is gratefully acknowledged. Support by the Ministry of Energy to A.N. is acknowledged.

-
- [1] E. A. Sedov, K. P. Riikonen, and K. Yu, *npj Quantum Mater.* **2**, 18 (2017).
- [2] T. Hirahara, T. Nagao, I. Matsuda, G. Bihlmayer, E. V. Chulkov, Y. M. Koroteev, and S. Hasegawa, *Phys. Rev. B* **75**, 035422 (2007).
- [3] S. Ito, B. Feng, M. Arita, A. Takayama, R.-Y. Liu, T. Someya, W.-C. Chen, T. Iimori, H. Namatame, M. Taniguchi, C.-M. Cheng, S.-J. Tang, F. Komori, K. Kobayashi, T.-C. Chiang, and I. Matsuda, *Phys. Rev. Lett.* **117**, 236402 (2016).
- [4] S. Ito, M. Arita, J. Haruyama, B. Feng, W.-C. Chen, H. Namatame, M. Taniguchi, C.-M. Cheng, G. Bian, S.-J. Tang, T.-C. Chiang, O. Sugino, F. Komori, and I. Matsuda, *Sci. Adv.* **6**, eaaz5015 (2020).
- [5] R. Hartman, *Phys. Rev.* **181**, 1070 (1969).
- [6] Y. Yafet, *Solid State Physics*, 5th ed. (Academic Press, New York, 1963), Vol. 14.
- [7] N. Marcano, S. Sangiao, C. Magén, L. Morellón, M. R. Ibarra, M. Plaza, L. Pérez, and J. M. De Teresa, *Phys. Rev. B* **82**, 125326 (2010).
- [8] X. Sun, Z. Zhang, and M. S. Dresselhaus, *Appl. Phys. Lett.* **74**, 4005 (1999).
- [9] Y. Ohtsubo, L. Perfetti, M.-O. Goerbig, P. L. Fèvre, F. Bertran, and A. Taleb-Ibrahimi, *New J. Phys.* **15**, 033041 (2013).
- [10] H. M. Benia, C. Straßer, K. Kern, and C. R. Ast, *Phys. Rev. B* **91**, 161406(R) (2015).
- [11] F. Gity, L. Ansari, M. Lanius, P. Schüffelgen, G. Mussler, D. Grützmacher, and J. C. Greer, *Appl. Phys. Lett.* **110**, 093111 (2017).
- [12] S. Xiao, D. Wei, and X. Jin, *Phys. Rev. Lett.* **109**, 166805 (2012).
- [13] K. Zhu, L. Wu, X. Gong, S. Xiao, and X. Jin, *Phys. Rev. B* **94**, 121401(R) (2016).
- [14] P. Kröger, D. Abdelbarey, M. Siemens, D. Lükermann, S. Sologub, H. Pfnür, and C. Tegenkamp, *Phys. Rev. B* **97**, 045403 (2018).
- [15] H. Ishida, *J. Phys.: Condens. Matter* **29**, 015002 (2018).
- [16] Yu. M. Koroteev, G. Bihlmayer, J. E. Gayone, E. V. Chulkov, S. Blügel, P. M. Echenique, and Ph. Hofmann, *Phys. Rev. Lett.* **93**, 046403 (2004).
- [17] D. Lükermann, S. Sologub, H. Pfnür, and C. Tegenkamp, *Phys. Rev. B* **83**, 245425 (2011).
- [18] N. Miyata, R. Hobara, H. Narita, T. Hirahara, S. Hasegawa, and I. Matsuda, *Jpn. J. Appl. Phys.* **50**, 036602 (2011).
- [19] T. Hirahara, I. Matsuda, S. Yamazaki, N. Miyata, and S. Hasegawa, *Appl. Phys. Lett.* **91**, 202106 (2007).
- [20] M. Aitani, T. Hirahara, S. Ichinokura, M. Hanaduka, D. Shin, and S. Hasegawa, *Phys. Rev. Lett.* **113**, 206802 (2014).
- [21] D. Abdelbarey, J. Koch, Z. Mamiyev, C. Tegenkamp, and H. Pfnür, *Phys. Rev. B* **102**, 115409 (2020).
- [22] J. S. Kim, S. S. A. Seo, M. F. Chisholm, R. K. Kremer, H.-U. Habermeier, B. Keimer, and H. N. Lee, *Phys. Rev. B* **82**, 201407(R) (2010).
- [23] Z. Ren, A. A. Taskin, S. Sasaki, K. Segawa, and Y. Ando, *Phys. Rev. B* **82**, 241306(R) (2010).
- [24] P. Ngabonziza, Y. Wang, and A. Brinkman, *Phys. Rev. Mater.* **2**, 044204 (2018).
- [25] G. Cantele and D. Ninno, *Phys. Rev. Mater.* **1**, 014002 (2017).
- [26] V. Madhavan, W. Chen, T. Jamneala, M. F. Crommie, and N. S. Wingreen, *Science* **280**, 567 (1998).
- [27] J. Göres, D. Goldhaber-Gordon, S. Heemeyer, M. A. Kastner, H. Shtrikman, D. Mahalu, and U. Meirav, *Phys. Rev. B* **62**, 2188 (2000).
- [28] A. C. Johnson, C. M. Marcus, M. P. Hanson, and A. C. Gossard, *Phys. Rev. Lett.* **93**, 106803 (2004).
- [29] K. Kobayashi, H. Aikawa, S. Katsumoto, and Y. Iye, *Phys. Rev. Lett.* **88**, 256806 (2002).

- [30] K. Kobayashi, H. Aikawa, S. Katsumoto, and Y. Iye, *Phys. Rev. B* **68**, 235304 (2003).
- [31] J. Kim, J.-R. Kim, J.-O. Lee, J. W. Park, H. M. So, N. Kim, K. Kang, K.-H. Yoo, and J.-J. Kim, *Phys. Rev. Lett.* **90**, 166403 (2003).
- [32] S. Norimoto, S. Nakamura, Y. Okazaki, T. Arakawa, K. Asano, K. Onomitsu, K. Kobayashi, and N.-h Kaneko, *Phys. Rev. B* **97**, 195313 (2018).
- [33] S. Wang, B.-C. Lin, W.-Z. Zheng, D. Yu, and Z. M. Liao, *Phys. Rev. Lett.* **120**, 257701 (2018).
- [34] A. Schuray, L. Weithofer, and P. Recher, *Phys. Rev. B* **96**, 085417 (2017).
- [35] J. U. Nöckel and A. D. Stone, *Phys. Rev. B* **50**, 17415 (1994).
- [36] J. G. Rodrigo, A. García-Martín, J. J. Sáenz, and S. Vieira, *Phys. Rev. Lett.* **88**, 246801 (2002).
- [37] H. F. Pernau, T. Pietsch, and E. J. Scheer, *J. Phys.: Condens. Matter* **26**, 474203 (2014).
- [38] C. Sabater, D. Gosálbez-Martínez, J. Fernández-Rossier, J. G. Rodrigo, C. Untiedt, and J. J. Palacios, *Phys. Rev. Lett.* **110**, 176802 (2013).
- [39] P. G. Silvestrov and Y. Imry, *Phys. Rev. Lett.* **85**, 2565 (2000).
- [40] C. Karrasch, T. Hecht, A. Weichselbaum, Y. Oreg, J. von Delft, and V. Meden, *Phys. Rev. Lett.* **98**, 186802 (2007).
- [41] M. Goldstein, R. Berkovits, Y. Gefen, and H. A. Weidenmüller, *Phys. Rev. B* **79**, 125307 (2009).
- [42] M. Müller and I. Rotter, *Phys. Rev. A* **80**, 042705 (2009).
- [43] E. Shapira, A. Holtzman, D. Marchak, and Y. Selzer, *Nano Lett.* **12**, 808 (2012).
- [44] Z. Zhang, X. Sun, M. S. Dresselhaus, J. Y. Ying, and J. Heremans, *Phys. Rev. B* **61**, 4850 (2000).
- [45] M. Neklyudova, C. Sabater, A. K. Erdamar, J. M. van Ruitenbeek, and H. W. Zandbergen, *Appl. Phys. Lett.* **110**, 103101 (2017).
- [46] See Supplemental Material at <http://link.aps.org/supplemental/10.1103/PhysRevB.104.235140> for details on the characterization of the Ohmic contacts and on the calculations of the density of states.
- [47] Y.-M. Lin, X. Sun, and M. S. Dresselhaus, *Phys. Rev. B* **62**, 4610 (2000).
- [48] V. V. Enaldiev and V. A. Volkov, *Phys. Rev. B* **97**, 115305 (2018).
- [49] V. Tinnemann, C. Streubühr, B. Hafke, A. Kalus, A. Hanisch-Blicharski, M. Ligges, P. Zhou, D. von der Linde, U. Bovensiepen, and M. Horn-von Hoegen, *Struct. Dyn.* **6**, 035101 (2019).
- [50] H. Steinberg, J. B. Laloë, V. Fatemi, J. S. Moodera, and P. Jarillo-Herrero, *Phys. Rev. B* **84**, 233101 (2011).
- [51] A. Avinun-Kalish, M. Heiblum, O. Zarchin, D. Mahalu, and V. Umansky, *Nature (London)* **436**, 529 (2005).
- [52] A. I. Magunov, I. Rotter, and S. I. Strakhova, *Phys. Rev. B* **68**, 245305 (2003).
- [53] A. Boukai, K. Xu, and J. R. Heath, *Adv. Mater.* **18**, 864 (2006).
- [54] M. Goldstein, R. Berkovits, and Y. Gefen, *Phys. Rev. Lett.* **104**, 226805 (2010).
- [55] F. Borsoi, K. Zuo, S. Gazibegovic, R. L. M. Op het Veld, E. P. A. M. Bakkers, L. P. Kouwenhoven, and S. Heedt, *Nat. Commun.* **11**, 3666 (2020).
- [56] T. E. Huber, A. Adeyeye, A. Nikolaeva, L. Konopko, R. C. Johnson, and M. J. Graf, *Phys. Rev. B* **83**, 235414 (2011).
- [57] L. A. Konopko, T. E. Huber, A. A. Nikolaeva, and L. A. Borceacov, *J. Low Temp. Phys.* **171**, 677 (2013).
- [58] A. Nikolaeva, D. Gitsu, L. Konopko, M. J. Graf, and T. E. Huber, *Phys. Rev. B* **77**, 075332 (2008).
- [59] L. Ansari, F. Gity, and J. C. Greer, *J. Phys.: Condens. Matter* **29**, 065301 (2017).
- [60] C. König, S. Fahy, and J. C. Greer, *Phys. Rev. Mater.* **3**, 065002 (2019).
- [61] V. M. Garcia-Suarez, R. Ferradas, and J. Ferrer, *Phys. Rev. B* **88**, 235417 (2013).
- [62] G. Bevilacqua, G. Grosso, G. Menichetti, and G. Pastori Parravicini, *Phys. Rev. B* **94**, 245419 (2016).